Communication

Atomic-Scale Structural and Magnetic Coupling Properties of Twin Boundaries in LiFe5O8 Film

Kun Liu *, Jiankang Li , Songyou Zhang

Posted Date: 19 June 2024

doi: 10.20944/preprints202406.1300.v1

Keywords: lithium ferrite; twin boundaries; magnetic; electron microscopy

 doi:10.20944/preprints202406.1300.v1

Communication

Atomic-Scale Structural and Magnetic Coupling Properties of Twin Boundaries in $LiFe_5O_8$ Film

Kun Liu *, Jiankang Li and Songyou Zhang

School of Electronics and Information Engineering, Suzhou Vocational University, Suzhou 215104, China; ljk@jssvc.edu.cn (J.L.); 92207@jssvc.edu.cn (S.Z.)
* Correspondence: 92107@jssvc.edu.cn

Abstract: It is of great academic significance to understand how the atomic structure of interfaces and boundaries in materials impacts the magnetic coupling nature across the boundaries and encourage development of state-of-the-art magnetic devices. Here, we carry out a systematic investigation of the atomic and electronic structures of twin boundaries (TBs) in $LiFe_5O_8$ thin films and determine their concurrent magnetic couplings using atomic-resolution transmission electron microscopy and atomistic first-principles calculations. The results show ferromagnetic or antiferromagnetic coupling can exist across the different TBs in $LiFe_5O_8$ (LFO) thin films and electrical structures within a few atomic layers directly rely on the TB atomic core structures. Uncovering one-to-one relationship between the magnetic properties of individual TB and the local atomic structures will clarify a thorough comprehension of numerous fascinating magnetic properties of commonly utilized magnetic materials, which will undoubtedly encourage the progress of sophisticated magnetic materials and devices.

Keywords: lithium ferrite; twin boundaries; magnetic; electron microscopy

1. Introduction

A wide range of magnetic properties can be found in spinel ferrites, which have drawn attention for potential utilization in sensors, transformers, antennas, high-frequency inductors, microwave devices and spintronic devices [1]. Magnetic coupling across boundaries in spinel ferrites plays a critical role in both fundamental research significance and magnetic application. For instance, antiphase boundaries (APBs) have been frequently observed in spinel ferrite films, e.g., Fe_3O_4, $NiFe_2O_4$, and LFO [2–4]. Atomic models and magnetic coupling across APBs have been extensively determined using high resolution scanning transmission electron microscopy (STEM) and density function theory in spinel-type materials [5–7]. Antiferromagnetic coupling occurs across the APBs, leading to non-saturation of magnetization and larger magnetoresistance of the ferromagnetic film, which can be harmful for applications [8–10]. In contrast, engineering the formation of APBs have emerged as a promising approach to effectively modulate the functionality in solid oxide fuel applications [11]. Therefore, it is vital to understand atomic structure configurations and magnetic coupling across individual boundaries to tailor the magnetic properties. However, the challenges of simultaneously and accurately determining the atomic structure and magnetic coupling of individual boundaries severely hamper efforts to study the relationship between local atomic structures and magnetic coupling of boundaries. This is a fascinating but difficult research topic in interface and boundary science.

Besides APBs, TBs were found in spinel-type materials, e.g., Fe_3O_4 and $CoFe_2O_4$, which exhibit the abnormal magnetic properties [11]. The controllable formation of TBs in spinel lithium manganate help to obtain a higher rate performance [12]. In particular, Chen et al. have reported that atomic configuration and magnetic coupling of TBs in Fe_3O_4 single crystal by combination of STEM and differential phase contrast (DPC) imaging technique, suggesting that ferromagnetic or antiferromagnetic coupling of TBs in Fe_3O_4 are related to the atomic cores of the TBs, e.g., the

 doi:10.20944/preprints202406.1300.v1

antiferromagnetic coupling across the non-stoichiometric TBs [14]. Remarkably, atomic structure models of TBs have been constructed on the basis of crystallographic relationships and verified experimentally using high-resolution STEM in LFO film grown on $SrTiO_3$ (STO) (001) substrate [15]. LFO being an abundant magnetic material attracts extensive attention due to its intriguing electronic and magnetic properties. Compared to Fe_3O_4 materials, non-magnetic Li ions instead of magnetic Fe ions are half occupied at octahedral sites, hence, the magnetic couplings associated with the TBs in LFO film remain unclear.

In present work, atomic structure configuration and magnetic coupling across TBs in LFO films grown on STO substrate have been investigated by combining atomic-resolution STEM and atomistic first-principles calculations, demonstrating that the magnetic coupling across the TBs can be either antiferromagnetic (AFM) or ferromagnetic (FM) dependent on atomic core structures and resultant electronic structures of the TBs.

2. Materials and Methods

The $LiFe_5O_8$ ceramic target for film growth was prepared by a standard solid-state reaction method with the initial reactants Fe_2O_3 and $LiCO_3$ (ratio 5:2) [16]. The LFO films were grown on single-crystalline STO (001) substrates by a high-pressure sputtering system at the substrate temperature of 800℃ and under 0.5 mbar of the mixed ambient of Ar and O_2 at the ratio of 1:1. Cross-sectional lamella specimens for TEM/STEM investigation were prepared by focused ion beam (FIB) lift-out technique using an FEI Helios600i Dualbeam system. The lamellae were cut in STO <110> orientations. Bright-field (BF) TEM images and selected-area electron diffraction (SAED) patterns were obtained on a JEOL JEM-2100 microscope. Atomic-resolution high angle annular dark field (HAADF) and annular bright field (ABF) images were acquired on a JEOL ARM200F with a probe aberration corrector, operated at 200 kV. In STEM mode a probe size of 0.1 nm at semi-convergence angle of α=22 mrad was used for HAADF and ABF imaging experiments. The HAADF and ABF detectors covered angular ranges of 90–176 mrads and 11–22 mrads, respectively.

The calculations of density functional theory are done with the projector augmented plane-wave basis, which is implemented in Vienna ab-initio simulation package [17]. And the plane-waves are cut-off at 400 eV. The exchange-correlations of electrons are described by the generalized gradient approximations with the form proposed by Perdew, Burke, and Ernzerhof [18]. The energy converge criterion for solving self-consistent Kohn-Sham equations is 10-5 eV. The Brillouin zone is sampled with resolutions better than 0.03 Å-1, using the scheme of Monkhorst-Pack [19]. To improve the descriptions on the strong electron-electron interactions in d-shells, DFT+U approach [20] is adopted with Ueff=3.8 eV on the d-shells of Fe ions. All the structures in this study are fully relaxed until the Hellman-Feynman smaller than 0.05 eV/Å. The formation energy of twin boundaries is defined as:

$$E_f = \frac{1}{2A}(E_{TB} - n_O\mu_O - n_{Fe}\mu_{Fe} - n_{Li}\mu_{Li}) \quad (1)$$

where E_{TB} is the total energy of the supercell model with two identical twin boundaries, n_O, n_{Fe}, and n_{Li} are the quantities of O, Fe, and Li ions in the supercell model, μ_{Fe} and μ_{Li} are the chemical potentials of Fe and Li ions which are defined to be the energy per one atom in the pure metal body centered crystals, μ_O is the chemical potential of O ions and it is calculated via the equation $8\mu_O+5\mu_{Fe}+\mu_{Li}=\mu(LiFe_5O_8)$ in which $\mu(LiFe_5O_8)$ is the energy of the cell of Li-doped Fe_3O_4, A denotes the area of each twin boundary.

3. Results and Discussions

Figure 1a displays the low magnification bright field (BF) TEM images of LFO thin film with the thickness of 30 nm, showing the cross-sectional overview of LFO/STO (001) heterosystem. The contrast difference between film and substrate is clearly visible and the film-substrate interface is marked by horizontal arrow. The oblique contrast lines indicated by yellow arrow are discerned in film and the contrast lines result from the twin boundaries, lying in (111) habit plane.

Figure 1b displays the typical diffraction patterns of the film, covering the LFO film and part of the STO substrate, recorded along the [1$\bar{1}$0] zone axis of STO. The diffraction patterns marked by

 doi:10.20944/preprints202406.1300.v1

yellow solid and yellow dashed rectangle results from the LFO matrix and twin domain area, respectively, also confirming that the twin boundaries lie in (111) habit plane. It is observed that the reflection spots split between film and substrate along in plane and out of plane, indicating that misfit strain relaxation occurs. Taking the lattice parameter of STO substrate (0.3905 nm) [21] as the calibration standard, in plane and out of plane lattice parameter of the film is calculated to be 0.8301 nm and 0.8359 nm, respectively.

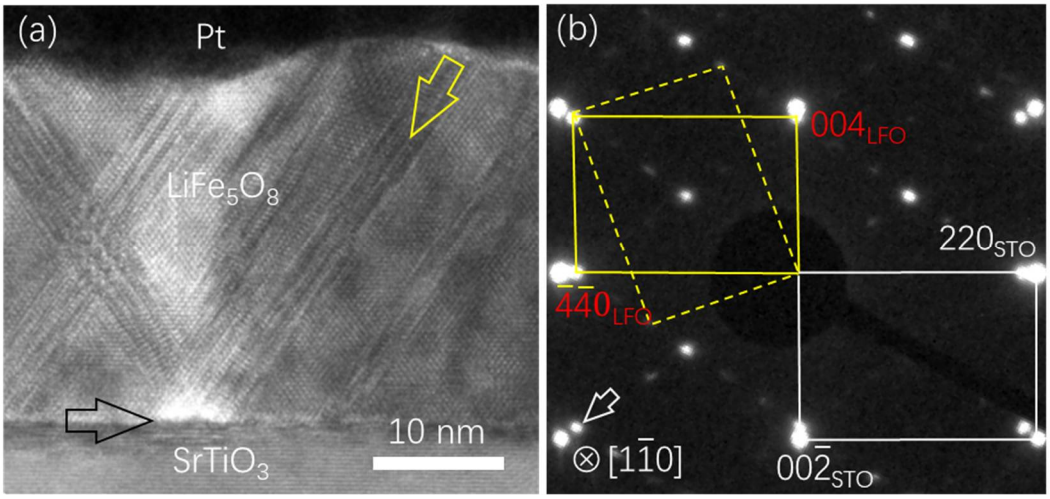

Figure 1. (a) Low-magnification BF-TEM images of a LFO film of 30 nm on STO (001) substrate. The film-substrate interface is indicated by a horizontal black arrow. (b) The typical SAED patterns of the LFO/STO (001) system 30nm, recorded along the [1$\bar{1}$0] STO zone axes. The splitting of the reflection spots is indicated by white oblique arrow.

High resolution STEM experiments have been performed to clearly identify the atomic structure of TBs viewed along [1$\bar{1}$0] zone axis of STO substrate. Numerous STEM observations show that three different types of twin boundaries coexist in LFO film at the same time. Figure 2 displays that three group of STEM-HAADF and ABF images of TBs, in which green, blue and red arrows in Figure 2 denote the boundaries of TB I, TB II and TB III, respectively. It is well-known that the intensity in HAADF image directly depends on the atomic number (Z) [22], as a result, the heavier atoms appear brighter, additionally, the higher atomic density will also generate the brighter contrast. Only the Fe atomic columns are visible in the HAADF images in Figure 2, while O columns are invisible due to much weaker scattering. The contrast difference of cation columns results from the different Fe atom density in [1$\bar{1}$0] projection direction. It is obvious that the cation arrangement of TB I is symmetric, in contrast, those of TB II and TB III are asymmetric, and three types of TBs all lie in (111) habit planes. Remarkably, TB III presents cation deficiency which induces intensity variation in atomic columns as marked by a red arrow in Figure 2(e). The white arrow demonstrates the atomic column with cation deficiency in Figure 2(e).

Figure 2 (b, d, f) display ABF images of three types of TBs simultaneously acquired with the corresponding HAADF image to immediately resolve O atom columns. According to ABF images, the oxygen sublattices in three types of TBs appear a feature of ∑3[111] coherent TBs. The twin planes of the TBs lie at O atom plane marked by green, blue and red arrows, respectively. Different cations arrangements in the O sublattices induce the formation of three different types of TBs which have been analyzed deeply in our previous works [15].

 doi:10.20944/preprints202406.1300.v1

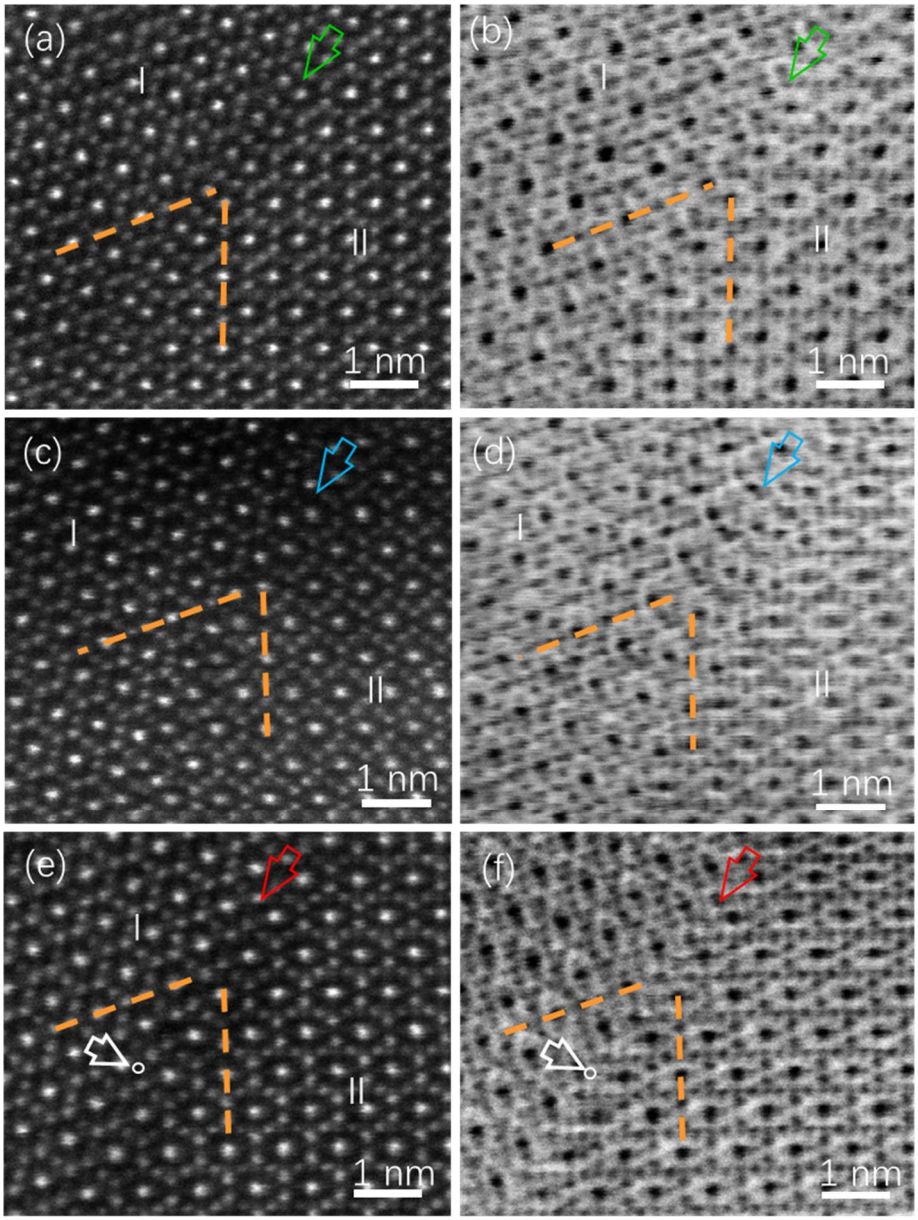

Figure 2. Clarifying atomic-scale structure of three types of TBs from the [1$\bar{1}$0] projection. (a, c, e) HAADF STEM images showing atomic structure of the type I, II, and III TBs, respectively. (b, d, f) Corresponding ABF STEM images showing atomic structure of these three types of TBs, which were taken simultaneously with the HAADF images and revealed all the atomic columns at the TBs including O. The white solid circles in (e) and (f) represent Fe vacancies.

To identify the magnetic properties of three types of TBs, density functional theory (DFT) computations were performed. On basis of the experimental STEM images, the potential candidate atomic models of TBs are established and the most energetically stable atomic structures were acquired in which formation energy is adopted. The formation energies of TB I, II, and III were determined to be 1.67 J/m^2, 0.75 J/m^2 and 2.80 J/m^2, respectively. However, the TB III was frequently observed in the LFO film, which is contradictory with the calculated formation energy. In fact, the APBs also form in LFO film, and APBs interact with TB I and TB II, further generate abundant TB III., which were frequently observed in previous work [15]. The density distribution of three types of TBs is different from that in Fe_3O_4 single crystal [14]. The lowest-energy optimal atomic configuration after relaxation were shown in Figure 3(a, c, e), STEM simulations were undertaken by use of the relaxed atomic models displayed in Figure 3(b, d, f), which matches well with the experimental counterparts.

 doi:10.20944/preprints202406.1300.v1

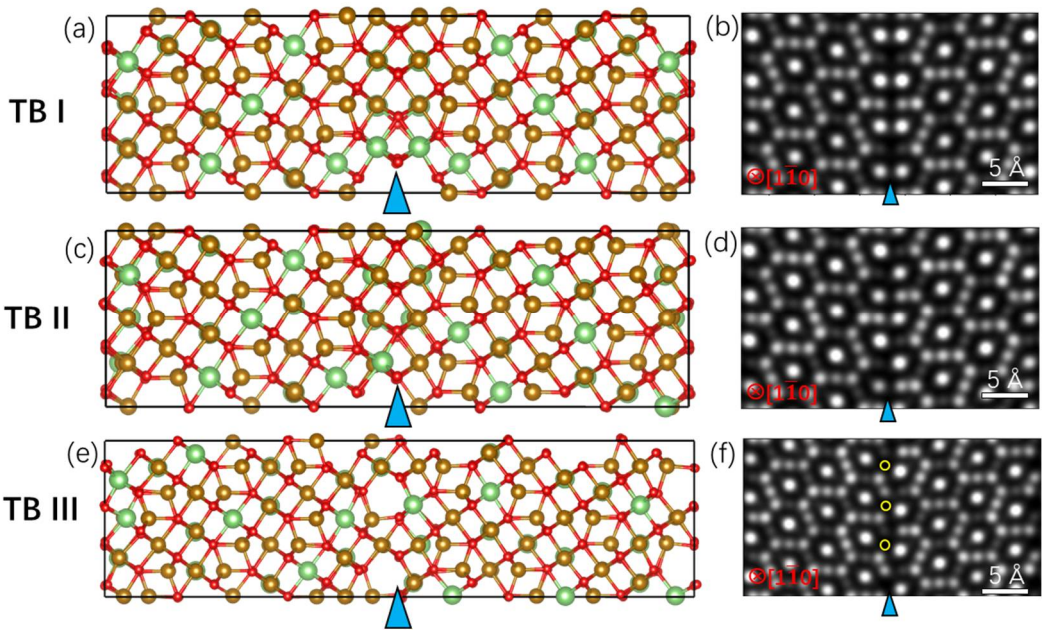

Figure 3. (a, c, e) The optimized atomic models of TB I, TB II and TB III, the vertical arrows denote the boundary of TB, (b, d, f) Simulated HAADF STEM images of three types of TBs along the [1$\bar{1}$0] zone axis. HAADF STEM images showing atomic structure of type I, II, and III TBs, respectively.

To determine the most stable magnetic configuration of each type of TBs, we compare the energy of FM and AFM coupling configuration. The results indicate that TB I prefer to configure as AFM coupling across the boundary with the interface formation energy 0.39 J/m^2 lower than that of FM coupling. Also, TB II configures preferably as AFM coupling across the boundary with interface formation energy 0.47 J/m^2 lower than that of FM coupling. In contrast, TB III typically develops FM couplings across boundaries with the interface formation energy -0.06 J/m^2 lower than that of AFM coupling. The weak FM coupling at TB III is likely to result from the Fe cation deficiency, which leads to the decreased density of super-exchange interactions between cations via oxygens [23].

The results of spin-polarized density of states (DOS) provides additional evidence of these magnetic coupling for TBs. As shown in Figure 4(a), the spin polarization flips direction across the boundary planes of the TB I, which suggests AFM coupling between two twin domains separated by TB I. The same situation appears in Figure 4(b), demonstrating AFM coupling nature at TB II. In strong contrast to DOS results of TB I and II, the spin polarization remains in the same direction across the boundary plane of TB III in Figure 4(c). Noticeably, the spin-polarized DOS at the three different types of TBs is directly depicted in Supplementary Figure S1, the spin polarization eventually inverts over the core area of TB I and II, revealing their AFM coupling nature. While, the direction of spin polarization keeps unaltered across the core region of TB III, which is consistent with its FM coupling nature.

Preprints.org (www.preprints.org) | NOT PEER-REVIEWED | Posted: 19 June 2024 doi:10.20944/preprints202406.1300.v1

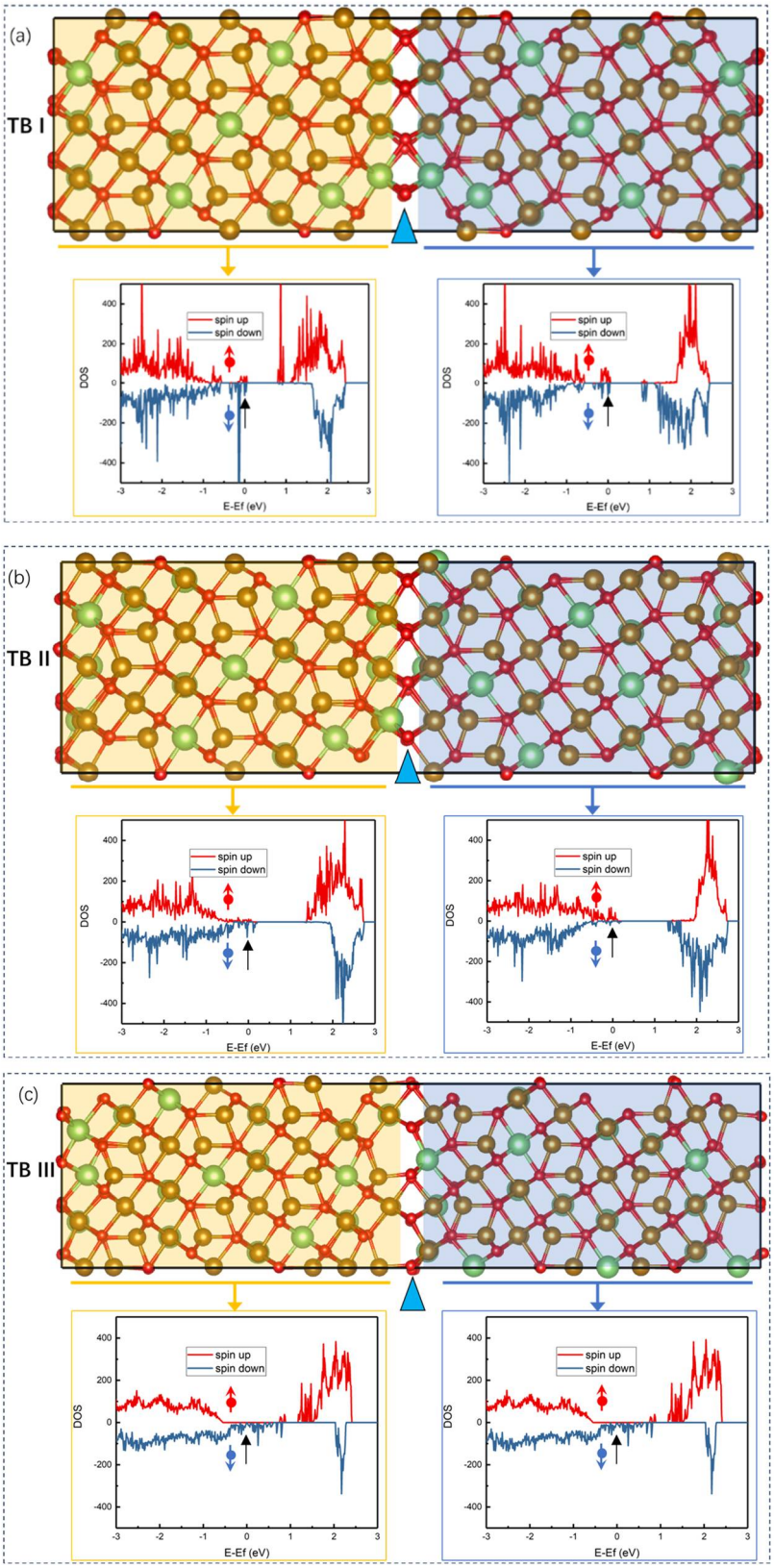

Figure 4. Spin-polarized DOS plots of TB I, TB II and TB III, the atoms within and near the boundary are indicated by colored shading. The relaxed atomistic models are also given for reference.

The atomic structures of three types of TBs in LFO film are similar with that in Fe_3O_4 crystal. Whereas, the magnetic couplings across the TBs are quite different from the results in Fe_3O_4 crystal, where the TB I and II both exhibit FM coupling and TB III have AFM coupling [12]. It is recognized

 doi:10.20944/preprints202406.1300.v1

that, in the spinel structure AB_2O_4, the magnetic spins align antiparallelly between the tetrahedral and the octahedral sites. Concerning magnetic coupling depending on super-exchange interaction via cation-oxygen-cation, bond angle should be considered. In contrast, the bond angles of 131.6°, 133.5°and 89.7° between A-O-B atoms dominates across the TB I, TB II and TBIII, respectively, acquired from relaxed atomic models. Particularly, B-site Li ions being not magnetic ions in LFO, the B-site occupation of Li ions at TB I and II is inclined to decrease FM exchange interactions between B-O-B atoms, which may result in the AFM coupling across TB I and II. On the contrary, the Fe deficiency exists at TB III, the antiferromagnetic super-exchange interactions between A-O-B atoms decrease, which results in that weak FM coupling are dominated at TB III. In present study, we predicted the ferromagnetic or antiferromagnetic coupling of TBs in LFO film by first-principles calculations, furthermore, direct experimental evidence for the magnetic coupling will be provided in future work to verify the DFT results. Considering the magnetic coupling across TBs in LFO, the nano-scale TBs, may have promising applications in nano-spintronic devices, e.g., spin torque magnetic random-access memory

4. Conclusion

In conclusion, understanding the interaction mechanism of atomic structure and magnetic coupling is crucial for the field of materials science. By combination of atomic-resolution STEM measurements and atomistic first-principles computations, we have successfully determined the atomic structure and magnetic coupling of different TBs in LFO films. It was discovered that the atomic core structure of TBs directly affects whether the magnetic coupling across the TBs is antiferromagnetic or ferromagnetic. Revealing the nature of the magnetic coupling across grain boundaries, as well as the material interfaces can help with the development of improved magnetic materials and technologies.

Supplementary Materials: The following supporting information can be downloaded at the website of this paper posted on Preprints.org.

Author Contributions: Conceptualisation, K.L.; investigation, K.L, S.Z.; writing—original draft preparation, K.L.; writing—review and editing, J.L, S.Z.; supervision, J.L. All authors have read and agreed to the published version of the manuscript.

Funding: This research was funded by the Natural Science Foundation of the Jiangsu Higher Education Institutions of China (Grant: 23KJB510032), the Enterprise practice of young teachers in vocational colleges in Jiangsu Province (2024QYSJ088), the Cultivation project of Suzhou vocational University (SVU2021py02), the Science and Technology Planning Project of Suzhou City (No. SZS2022015) and Jiangsu Provincial Universities "Qing-Lan Project".

Institutional Review Board Statement: Not applicable.

Informed Consent Statement: Not applicable.

Data Availability Statement: Not applicable.

Conflicts of Interest: The authors declare no conflict of interest.

References

1. Sanchez-Lievanos, K.R.; Stair, J.L.; Knowles, K.E.; Cation Distribution in Spinel Ferrite Nanocrystals: Characterization, Impact on their Physical Properties, and Opportunities for Synthetic Control. *Inorg. Chem.* **2021**, 60(7), 4291-4305.
2. McKenna, K.P.; Hofer, F.; Gilks, D.; Lazarov, V.K.; Chen, C.; Wang, Z.; Ikuhara, Y. Atomic-scale Structure and Properties of Highly Stable Antiphase Boundary Defects in Fe_3O_4, *Nat. Commun.* **2014,** 5, 5740.
3. Mi, S.B.; Zhang, R.Y; Lu, L.; Liu, M.; Wang, H.; Jia, C.L. Atomic-scale Structure and Formation of Antiphase Boundaries in α-$Li_{0.5}Fe_{2.5}O_4$ Thin Films on $MgAl_2O_4$(001) Substrates. *Acta Mater.* **2017,** 127, 178-184.
4. Singh, A.V.; Khodadadi, B.; Mohammadi, J.B.; Keshavarz, S.; Mewes, T.; Negi, D.S.; Datta, R.; Galazka, Z.; Uecker, R.; Gupta, A. Bulk Single Crystal-Like Structural and Magnetic Characteristics of Epitaxial Spinel Ferrite Thin Films with Elimination of Antiphase Boundaries. *Adv. Mater.* **2017,** 29, 1701222.
5. Liu, X.; Wu, M.; Qu, K.; Gao, P.; Mi, W. Atomic-Scale Mechanism of Grain Boundary Effects on the Magnetic and Transport Properties of Fe3O4 Bicrystal Films. *ACS Appl. Mater. & Interfaces* **2021,** 13(5), 6889-6896.

 doi:10.20944/preprints202406.1300.v1

6. Li, Z.; Lu, J.; Jin, L.; Rusz, J.; Kocevski, V.; Yanagihara, H.; Kita, E.; Mayer, J.; Dunin-Borkowski, R.E.; Xiang, H.; Zhong, X. Atomic Structure and Electron Magnetic Circular Dichroism of Individual Rock Salt Structure Antiphase Boundaries in Spinel Ferrites. *Adv. Funct. Mater.* **2021,** 31(21), 2008306.
7. Gao, C.; Jiang, Y.; Yao, T.; Tao, A.; Yan, X.; Li, X.; Chen, C.; Ma, X.L.; Ye, H. Atomic Origin of Magnetic Coupling of Antiphase Boundaries in Magnetite Thin films. *J Mater. Sci. Technol.* **2022,** 107, 92-99.
8. Margulies, D.T.; Parker, F.T.; Rudee, M.L.; Spada, F.E.; Chapman, J.N.; Aitchison, P.R.; Berkowitz, A.E.; Origin of the Anomalous Magnetic Behavior in Single Crystal Fe_3O_4 Films. *Phys. Rev. Lett.* **1997,** 79(25), 5162-5165.
9. Xu, K.; Lin, T.; Rao, Y. et al. Direct Investigation of the Atomic Structure and Decreased Magnetism of Antiphase Boundaries in Garnet. *Nat Commun.* **2022,** 13, 3206.
10. Wu, H.C.; Abid, M.; Chun, B.S.; Ramos, R.; Mryasov, O.N.; Shvets, I.V. Probing One Antiferromagnetic Antiphase Boundary and Single Magnetite Domain Using Nanogap Contacts. *Nano Lett.* **2010,** 10(4), 1132-1136.
11. Xu, K.; Hung, S.W.; Si. W. et al. Topotactically Transformable Antiphase Boundaries with Enhanced Ionic Conductivity. *Nat Commun.* **2023,** 14, 73822.
12. Guo, Z.; Jiang, H.; Sun, X.; Li, X.; Liu, Z.; Zhang, J.; Luo, J.; Zhang, J.; Tao, X.S.; Ding, J.; Han, X.; Liu, R.; Chen, Y.; Hu, W. Ultrafast Non-Equilibrium Phase Transition Induced Twin Boundaries of Spinel Lithium Manganate. *Adv. Energy Mater.* **2024,** 14, 2302484.
13. Leung, G.W.; Vickers, M.E.; Yu, R.; Blamire, M.G.; Epitaxial Growth of Fe_3O_4 (111) on $SrTiO_3$ (001) Substrates. *J. Cryst. Growth* **2008,** 310(24), 5282-5286.
14. Chen, C.; Li, H; Seki, T.; Yin, D.; Sanchez-Santolino, G.; Inoue, K.; Shibata, N.; Ikuhara, Y. Direct Determination of Atomic Structure and Magnetic Coupling of Magnetite Twin Boundaries. ACS Nano **2018,** 12(3), 2662-2668.
15. Liu, K.; Zhang, R.; Lu, L.; Mi, S.; Liu, M.; Wang, H.; Wu, S.; Jia, C. Atomic-scale Investigation of Spinel $LiFe_5O_8$ Thin Films on $SrTiO_3$ (001) Substrates. *J Mater. Sci. Technol.* **2020,** 40, 31-38.
16. R. Zhang, M. Liu, L. Lu, S.-B. Mi, H. Wang, Strain-tunable magnetic properties of epitaxial lithium ferrite thin film on $MgAl_2O_4$ substrates, *J. Mater. Chem. C* **2015,** 3(21), 5598-5602.
17. Kresse, G.; Joubert, D. From Ultrasoft Pseudopotentials to the Projector Augmented-wave Method. *Phys. Rev. B* **1999,** 59(3), 1758-1775.
18. Perdew, J.P.; Burke, K.; Ernzerhof, M. Generalized Gradient Approximation Made Simple. *Phys. Rev. Lett.* **1996,** 77(18), 3865-3868.
19. Chadi, D.J. Special Points for Brillouin-zone Integrations. *Phys. Rev. B* **1977,** 16(4), 1746-1747.
20. Anisimov, V.I.; Zaanen, J.; Andersen, O.K. Band Theory and Mott insulators: Hubbard U instead of Stoner I. *Phys. Rev. B* **1991,** 44(3) 943-954.
21. Howard, S.A.; Yau, J.K.; Anderson, H.U. Structural Characteristics of $Sr_{1-x}La_xTi_{3+\delta}$ as a Function of Oxygen Partial Pressure at 1400 °C. *J. Appl. Phys.* **1989,** 65(4), 1492-1498.
22. Pennycook, S.J.; Boatner, L.A. Chemically Sensitive Structure-imaging with a Scanning Transmission Electron microscope, *Nature* **1988,** 336(6199), 565-567.
23. Desai, H.B., Tanna, A.R. (2021). Effect of Substitution on the Electric and Magnetic Properties of Ferrites. In: Bhargava, G.K., Bhardwaj, S., Singh, M., Batoo, K.M. (eds) Ferrites and Multiferroics. Engineering Materials. Springer, Singapore.